Quaternary Science Reviews 29 (2010) 2705–2718

Contents lists available at ScienceDirect

Quaternary Science Reviews

journal homepage: www.elsevier.com/locate/quascirev

Climatic interpretation of a 1.9 Ma environmental magnetic record of loess deposition and soil formation in the central eastern Pampas of Buenos Aires, Argentina

Clifford W. Heil Jr. [a,*], John W. King [a], Marcelo A. Zárate [b], Peter H. Schultz [c]

[a] Graduate School of Oceanography, University of Rhode Island, Narragansett, Rhode Island 02882, USA
[b] CONICET-FCEN-UNLPAM, Avenida Uruguay 151, 6300, Santa Rosa, La Pampa, Argentina
[c] Brown University, Department of Geological Science, Providence, Rhode Island 02912, USA

ARTICLE INFO

Article history:
Received 12 November 2009
Received in revised form
10 June 2010
Accepted 12 June 2010

ABSTRACT

Much of what we know about Quaternary climate has been learned from sedimentary records from the world's oceans. With the exception of the extensive studies of the Chinese loess/paleosol sequence and more recent studies of long lake records, there are few long terrestrial climate records, particularly from the southern hemisphere. The loess record of Argentina provides an important opportunity to further our understanding of climate change from a terrestrial environment, but its complexity and discontinuity have led to difficulty in formulating a climatological model of depositional and pedogenic processes. In this study, we present one of the longest and most continuous loess/loessoid records from the central eastern Pampas of Argentina. Our age model is based on optically stimulated luminescent dates and a paleomagnetic reversal stratigraphy and indicates a basal age around 1.9 Ma. Within the age model uncertainties, we characterize the environmental magnetic properties associated with loess deposition and soil formation with respect to wind patterns, moisture availability, and temperature. Major changes in magnetic grain size are linked to a differential northward shift of the subtropical high-pressure cell during glacial periods. We suggest that coarser (finer) magnetic grains correspond to weaker (stronger) glacial periods when the high-pressure cell is located in a more southerly (northerly) position and the source region is more proximal (distal) to our study area. An abrupt increase in the ultrafine-grained magnetic material around 0.9 Ma is related to an increase in moisture transport from the South Atlantic driven by an increase in summer sea surface temperatures at the mid-Pleistocene transition (~1 Ma). In addition to these grain size variations, there is a relative decrease in the amount of goethite compared to hematite beginning around 0.5 Ma, which has been related to the temperature increase observed after the mid-Brunhes Event (~450 ka) in the EPICA ice core temperature record. A more detailed comparison to insolation indicates that, for portions of the record, ferrimagnetic minerals are depleted during periods of low insolation. This result suggests that Argentine loess deposition and soil formation follows a model more similar to the Alaskan loess sequences than the Chinese loess sequences. Although further work is needed to validate the models and mechanisms proposed in this study, our record indicates that the mineral magnetic properties of the loess and paleosol deposits record major changes in deposition and soil formation and provide insight into possible mechanisms relating to global and/or hemispheric climate change.

1. Introduction

Among the most important terrestrial paleoclimate records are those from the loess and paleosol sequences of central China and the Tibetan Plateau (Heller and Liu, 1986; Kukla and An, 1989; Zhou et al., 1990; Maher and Thompson, 1995; Sun et al., 2006). Mineral magnetic studies of these sequences have demonstrated the complexity of preservation and/or formation of magnetic minerals during the pedogenic process as well as changes in loess deposition. These records have contributed significantly to our understanding of monsoonal circulation and its role in heat and moisture transport to Southeast Asia during the last ~8 Ma.

The loess/loessoid deposits of Argentina have the potential to be a southern hemisphere counterpart to the sequences of China. The loess/loessoid sediments of Argentina were deposited during glacial intervals by westerly winds carrying material from the

* Corresponding author. Tel.: +1 401 874 6537; fax: +1 401 874 6811.
E-mail address: chip@gso.uri.edu (C.W. Heil Jr.).

0277-3791/$ – see front matter © 2010 Elsevier Ltd. All rights reserved.
doi:10.1016/j.quascirev.2010.06.024

Andes Cordillera (Frenguelli, 1957; Teruggi, 1957; Bidegain et al., 2007). These sediments have accumulated since the late Miocene (~10 Ma; Zárate, 2003 and references therein) and contain discrete paleosols and/or pedogenic units (Bidegain, 1998; Nabel et al., 1999; Kemp and Zárate, 2000; Zinck and Sayago, 2001; Zárate et al., 2002; Zárate, 2003; Bidegain et al., 2005; Kemp et al., 2006; Schellenberger and Veit, 2006; Bidegain et al., 2007). However, many of these studies have shown that the loess/paleosol sequences of Argentina have been affected by compound pedogenesis, which creates a complex stratigraphy and obscures correlations to regional and global paleoclimate records. In addition, the sequences in Argentina contain hiatuses and erosional surfaces of unknown duration. Although these discontinuities do not appear to span long periods of time, they increase the complexity of the sequences.

Depending on the composition of the loess, iron (in both the Fe^{3+} and Fe^{2+} forms) can be liberated, mobilized, and ultimately bound with oxygen and/or hydrogen during weathering. The extent of weathering is determined by several environmental factors including temperature, water regime, pH, Eh (oxidation potential), biological activity, and the duration of exposure (Maher, 1986; Murad and Fischer, 1988). Two general magnetic depositional/pedogenic models have been established describing the mineral magnetic variations in loess/paleosol sequences. Briefly, the "wind vigor" model (i.e., Alaskan loess/paleosol sequence) is based on strong glacial winds carrying dense magnetic minerals in the loess material, whereas decreased wind strength and increased moisture during interglacial periods diminishes the concentration of magnetic minerals. The "pedogenic" model (i.e., Chinese loess/paleosol sequence) is based on magnetic enhancement of the parent loess during pedogenic interglacial intervals. Identifying the magnetoclimatological relationship in these types of environments is critical to constructing paleoclimate records and understanding them in the context of regional and global climate change.

In this paper we present a detailed (2 cm sample resolution) environmental magnetic characterization of six pedogenic units from a 16 m section located in the central eastern Pampas of Buenos Aires, Argentina. The age of the section was constrained using a magnetic reversal stratigraphy and optically stimulated luminescence dates (OSL) and spans the last ~1.9 Ma. We identified changes in magnetic concentration, mineralogy and grain size and related them to changes in available moisture, wind strength, and temperature. Ultimately, we consider our record in the context of global climate changes/patterns (e.g., orbital cycles, the mid-Pleistocene transition, and the Mid-Brunhes Event) and propose mechanisms to explain our observations.

2. Geologic setting

The Argentine Pampas extend from 23°S to 38°S in the southern plains of South America. Primarily derived from reworked pyroclastic deposits, primary tephra units, and other volcaniclastic sediments, the loess and loessoid/paleosol sequences span the Pliocene through the Pleistocene with similar underlying sequences extending to the late Tertiary (Zárate and Fasano, 1989; Schultz et al., 1998). Located 45 km southeast of the city of Buenos Aires, Gorina Quarry (34°54′08″S; 58°01′56″W) (Fig. 1) lies within the 'Pampa Ondulada' in the northeastern portion of the Argentine Pampas. The undulating topography formed by fluvial erosion associated with tributary streams of the Rio Paraná and Rio de la Plata (Zárate and Rabassa, 2005). The present climate is humid temperate, having a mean annual temperature of 17 °C and experiencing an average annual rainfall of 1000 mm (Prohaska, 1976). The section is composed primarily of clayey and sandy silts (Zárate et al., 2002) and has been divided by Bidegain (1998) into three

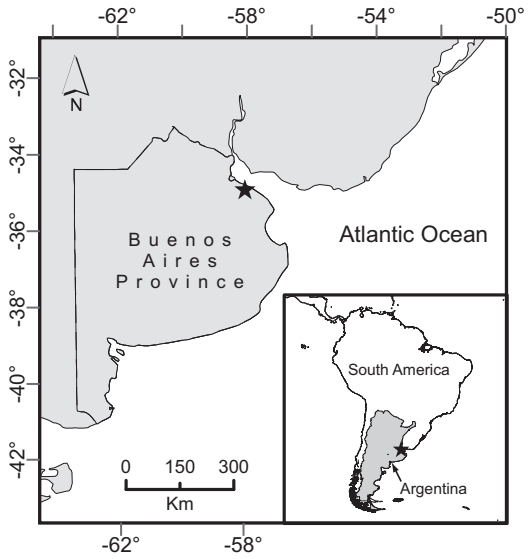

Fig. 1. Location map of Gorina Quarry, indicated by the star.

lithostratigraphic units: La Postrera Formation (youngest) (Fidalgo et al., 1973), the Buenos Aires Formation, and the Ensenada Formation (oldest) (Riggi et al., 1986). The Brunhes/Matuyama boundary (0.781 Ma) marks the upper boundary of the Ensenada Formation (Bidegain, 1998).

3. Methods

A series of 29 block samples (~8 cm deep × 8 cm across and ranging in length from 40 to 100 cm) were extracted from the southwest wall of Gorina Quarry. The exposed face of the outcrop was first cleared to remove weathered and/or slumped material. Maintaining an overlap of ~10 cm between the top and bottom of adjacent samples, a continuous 16 m section was recovered. In order to measure the paleomagnetic record (i.e., the magnetic reversal stratigraphy), a 2.5 cm × 2.5 cm continuous sub-sample was cut from the larger block samples. In addition to the continuous samples, discrete samples were taken every 2 cm from the block sections. Each discrete sample was ground into a powder and divided between two different sample containers (a 3.17 cm^3 plastic box and a 0.3 cm^3 plastic vial) and then weighed.

The natural remanent magnetization (NRM) was measured at 1 cm intervals along the continuous samples using a 2-$G_{®}$ Enterprises small-access cryogenic magnetometer. The samples were subjected to stepwise alternating field demagnetization at eight steps to a maximum of 30 mT, at which point the magnetization was typically less than 50% of its initial value. The NRM after demagnetization at a peak field of 20 mT is reported here. Demagnetization above this level produced linear demagnetization paths toward she origin (Suppl. Fig. 1).

Following the NRM measurements, a series of laboratory-induced magnetizations were performed on the 3.17 cm^3 and 0.3 cm^3 samples to characterize the concentration, size, and mineralogy of the magnetic minerals present in the sediment. Magnetic susceptibility (K or χ), anhysteretic remanent magnetization (ARM), and saturation isothermal remanent magnetization (SIRM) commonly reflect the content of ferrimagnetic minerals (e.g., magnetite, titanomagnetite, and greigite) but differ in their sensitivity to variations in magnetic grain size (Dunlop and Özdemir, 1997). These ferrimagnetic minerals are characteristically strongly magnetic and have relatively low coercivities. For

ferrimagnetic grains large enough to carry a remanent magnetization (≥30 nm), *K* has a weak dependence on magnetic grain size, increasing somewhat as grains increase from single domain to multi-domain. For such remanence-carrying grains, both SIRM and ARM decrease with increasing grain size so that large multi-domain grains contribute relatively little in comparison to smaller grains. In comparison to SIRM, ARM varies more strongly for very small grains (<1 μm), with ARM being particularly strong for magnetite grains with diameters on the order of 0.1 μm or smaller (King et al., 1982; Dunlop and Özdemir, 1997). Because of the differing dependence of these magnetic properties on the size of ferrimagnetic grains, the ratios ARM/*K*, SIRM/*K*, and ARM/SIRM provide convenient qualitative measures of "magnetic grain size" (with higher values indicating finer sizes) and are used in this study. Grain size interpretations based on these ratios assume that *K*, ARM, and SIRM reflect the same ferrimagnetic minerals. This assumption is commonly violated when *K* is significantly affected by superparamagnetic, paramagnetic and/or diamagnetic material, when SIRM contains a large high-coercivity component (e.g., hematite and goethite), and when there are major changes in the type of ferrimagnetic minerals.

In order to address the ambiguities with these grain size parameters, the sediment in the 3.17 cm^3 boxes was used to measure the high and low frequency mass magnetic susceptibility (χ_{lf} and χ_{hf}), frequency dependence of magnetic susceptibility (χ_{fd}%), and the ARM. χ_{lf} and χ_{hf} were measured using a Bartington Instruments MS2B dual frequency sensor (470 Hz and 4700 Hz). Each sample was measured 3 times at each frequency and the average values for χ_{lf} and χ_{hf} were used to calculate χ_{fd}% (defined as $[(\chi_{lf} - \chi_{hf})/\chi_{lf}] \times 100$). While χ and *K* are magnetic concentration parameters, χ_{fd}% is an indicator of the amount of superparamagnetic material (< ~25–30 nm; Dunlop and Özdemir, 1997) in the sediment. Both parameters have been used as indicators of pedogenesis related to rainfall and paleomonsoon intensity (Maher et al., 1994, 2002; Maher and Thompson, 1995; Chen et al., 1999; Deng et al., 2005).

To better characterize concentration changes and variations in the <1 μm size range, an ARM was imparted in a 100 mT peak alternating field while in the presence of a 79.6 A/m direct field. After measurement of the initial ARM, the samples were subjected to incremental alternating field demagnetization at fields of 10, 15, 20, 25, and 30 mT. It has been shown that the ratio of $ARM_{30\ mT}$/ARM provides a qualitative magnetic grain size proxy that can have a direct relationship to bulk grain size variations (Blanchet et al., 2007). We compare this proxy to the other well-established magnetic grain size proxies mentioned above.

The samples in the 0.3 cm^3 vials were subjected to a series of isothermal remanent magnetizations (IRM) using an ASC Scientific Model IM-10-30 Impulse Magnetizer to characterize changes in the amount of high-coercivity minerals. The premise behind these high-field treatments and measurements is that high-coercivity minerals (e.g., hematite and goethite) approach magnetic saturation in fields >1 T while low-coercivity minerals (e.g., magnetite and maghemite) saturate around 0.3 T. The remanent magnetization measured after removal from the saturating field is known as the saturation isothermal remanent magnetization (SIRM). Although the saturating fields for hematite and goethite are not well-known, and have been suggested to be in excess of 20 T (Rochette et al., 2005), we subjected our samples to a saturation field of 4.4 T (the largest field attained by the impulse magnetizer) and a back field of 0.3 T followed by a second back field of 2.5 T. Based on the approach of Sangode and Bloemendal (2004) who show that the maximum percentage of IRM acquisition for hematite and goethite occur between 0.5–1 T and 3–4 T, respectively, the IRM fields that we have chosen should result in a sufficiently distinct mineralogical saturation to characterize the relative contributions of low-coercivity minerals versus high-coercivity minerals as well as the relative contribution of hematite versus goethite.

The distinction between goethite and hematite is important because the goethite to goethite + hematite ratio [$G/(G + H)$] has been used to infer climatic phases of pedogenesis relating to temperature and moisture (e.g., Sangode and Bloemendal, 2004). In general, warmer temperatures favor hematite formation (i.e., lower ratio values) and higher excess moisture favors goethite formation (i.e., higher ratio values). However, the relationship is confounded by the combination of these climatic factors as well as soil pH and organic carbon content (Kämpf and Schwertmann, 1983). Following the sequential magnetizations and measurements, the *S*-ratio (defined here as $IRM_{-0.3\ T}/IRM_{4.4\ T}$), HIRM [defined here as $(IRM_{4.4\ T} - IRM_{-0.3\ T})/2$] and the goethite and hematite contents ($G = IRM_{4.4\ T} - IRM_{-2.5\ T}$; $H = IRM_{-2.5\ T} - IRM_{-0.3\ T}$) were calculated.

To further characterize the environmental magnetic changes, 5–20 mg samples were taken throughout the section (74 total samples with an average sample spacing of ~20-cm) and measured using a Princeton Measurements Corporation Alternating Gradient Magnetometer. The samples were measured to obtain the saturation remanent magnetization (M_{rs}), the saturation magnetization (M_s), the magnetic coercivity (H_c) and the coercivity of remanence (H_{cr}). We use H_{cr} and M_{rs}/M_s to characterize variations in the relative contribution of high-coercivity minerals (e.g., hematite and goethite) and magnetic grains size, respectively (Day et al., 1977). Like the interparametric ratios discussed above, higher values of M_{rs}/M_s indicate finer magnetic grain sizes.

4. Sedimentology

The Gorina sedimentary succession resulted from the accretion of coarse to fine aeolian dust and consists of six pedological units (Pu1–Pu6) identified on the basis of field morphological properties (Fig. 2). In addition, two erosional surfaces are observed near the bottom of Pu1 (the present surface soil and its parent loess) and at the bottom of Pu4 (Zárate et al., 2002, 2009). At field scale, the sequence is primarily divided into B and C horizons. Redoximorphic features (Fe mottles, Fe–Mn nodules) varying from rare to common are found from the lower section of Pu1 downward, whereas carbonate nodules occur throughout the section. Zárate et al. (2002) carried out a systematic micromorphological analysis of the upper five pedological units, suggesting that Pu4, Pu3 and Pu2 are accretionary or compound paleosols rather than discrete paleosols. Compound pedogenesis may have masked evidence for depositional hiatuses. A progressive grain size decrease occurs from the lower part of Pu4 upwards with a dominance of fine textured sediments in the upper three units (Blasi et al., 2001; Zárate et al., 2002). The very fine sand fraction of the upper five pedological units is lithologically heterogeneous, including not only volcanic but also metamorphic and granitic rock particles. Fresh volcanic glass occurs in low amounts throughout the section (slightly more abundant in the lower parts of Pu4 and Pu1); the clay mineral assemblage is composed of illite (dominant in Pu1, Pu4 and Pu5), smectite, interstratified illite–smectite (prevailing in Pu2) with traces of kaolinite throughout; the amounts of illite, smectite, and interstratified illite–smectite are about equal in Pu3 (Blasi et al., 2001).

One of the most notable features in the Gorina section is the general absence of A horizons. This absence is an important distinction between this section and other "typical" loess/paleosol sections (e.g., China and Alaska). Kemp and Zárate (2000) provide a pedogenic model to explain the absence of A horizons that calls for a period of landscape stability, during which time AE

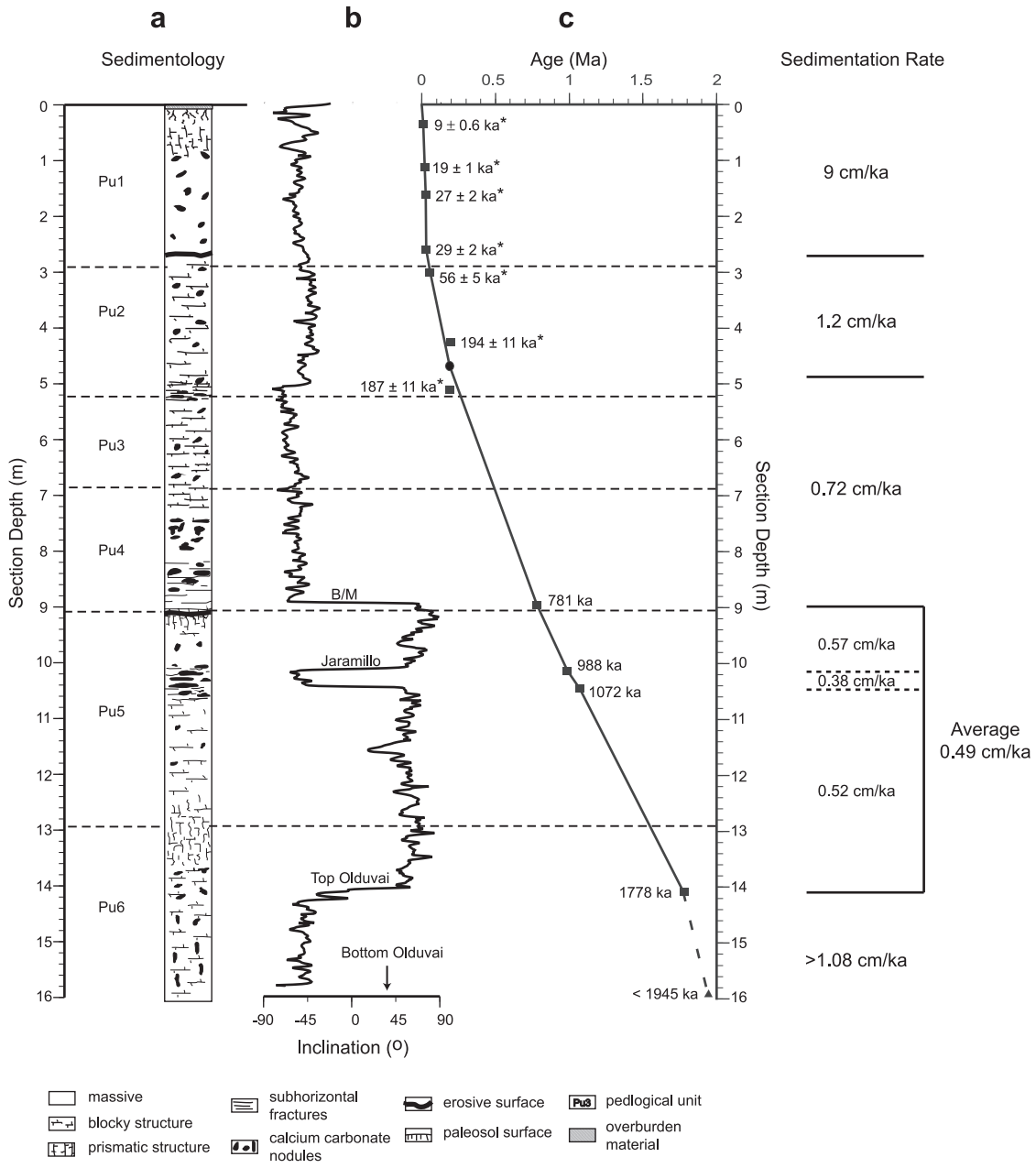

Fig. 2. (a) Sedimentological log showing paleosol units of Zárate et al. (2002). (b) Inclination record indicating reversal boundaries; Brunhes/Matuyama Boundary (B/M – 0.781 Ma), Jaramillo (0.988–1.072 Ma), Top Olduvai (1.778 Ma). Ages of reversal boundaries from Ogg and Smith (2004). (c) Age model based on optically stimulated luminescent dates (indicated with asterisks) of Zárate et al. (2009) and reversal boundaries. Average sedimentation rates are shown and the linear fit is discussed in the text. The closed circle at 190.5 ka and 4.675 m is the average age and depth of the inverted OSL dates discussed in Section 5.1.

and Bt horizons develop (e.g., the modern AE horizon formed during the Holocene), followed by a period of loess accumulation and pedogenesis that changes the AE horizon into BCt/AE horizons. The continued development of AE and Bt horizons and subsequent homogenization over several glacial/interglacial cycles results in pedologic units that lack discrete AE horizons. Although this model was developed for the Pliocene loess–paleosol sequence at Los Acantilados of east-central Argentina (Kemp and Zárate, 2000) and the Pleistocene loess–paleosol sequence at La Mesada in the Tucumán province of northwest Argentina (Kemp et al., 2003), it has been proposed as a suitable analog for the formation of pedologic units at Gorina Quarry (Zárate et al., 2002).

5. Results

5.1. Chronology and sedimentation rates

OSL ages were obtained to establish a chronology for the upper 5 m of the section (Zárate et al., 2009). The results indicate ages between 9 ± 0.6 ka in the lowermost part of the modern A horizon (0.35 m depth) to 29 ± 2 ka at the lower part of Pu1 (2.6 m, Fig. 2). In addition to these dates, OSL samples from the upper part of the Pu4–Pu3–Pu2 pedocomplex (2.95–8.3 m), with its upper limit reinterpreted based on a reevaluation of published data (Zárate et al., 2009), provided minimum age estimates of 56 ± 5 ka, 187 ± 11 ka, and 194 ± 11 ka at depths of 3.0, 5.1, and 4.25 m, respectively (Fig. 2)

A total of four paleomagnetic reversal boundaries were identified in the inclination data from the 16 m section at Gorina Quarry (Fig. 2). The uppermost ~9 m of the section records negative inclination values, indicating deposition during the Brunhes normal polarity chron. The transition to positive inclination values at 8.95 m is interpreted as the Brunhes–Matuyama boundary (781 ka; Ogg and Smith, 2004). Its position just above the Pu4/Pu5 paleosol boundary (Zárate et al., 2002) is consistent with previous studies at this locale (Bidegain, 1998). Three other reversal boundaries are identified below the B/M boundary. The brief interval of negative inclination values between 10.13 and 10.45 m is interpreted as the Jaramillo normal subchron (988–1072 ka; Ogg and Smith, 2004). The transition from positive inclination values to negative inclination values at 14.09 m is interpreted as the upper boundary of the Olduvai normal subchron (1778 ka; Ogg and Smith, 2004). The remainder of the section (14.09–15.85 m) records negative inclination values indicating that the lower boundary of the Olduvai subchron (1945 ka; Ogg and Smith, 2004) is not reached. This sequence of reversal boundaries suggests that the basal age for the Gorina Quarry section is <1945 ka.

The age model was constructed using a linear interpolation between OSL and reversal ages (Fig. 2). The two OSL dates at 5.1 and 4.25 m (187 and 194 ka, respectively) exhibit an age/depth inversion; however, they overlap in time within the error estimates (±11 ka each). In order to constrain the age for this interval, we have forced the age model through the average age and depth, 190.5 ka and 4.675 m, respectively (closed circle in Fig. 2). The interpolated ages below the upper Olduvai reversal (1778 ka) are maximum age estimates based on the absence of the lower Olduvai reversal (1945 ka) (Fig. 2). Based on this age model, there are four apparent changes in sediment accumulation rates for this section. The sediments of the lowermost interval (>1778 ka) must have accumulated at a rate >1.08 cm/ka since the lower Olduvai is not recovered in our samples. Between 1778 and 781 ka, the average sedimentation rate is ~0.49 cm/ka. This estimate may be low due to the presence of the erosional surface at the Pu4/Pu5 boundary, but it is notable that sediment accumulation decreased by 50% compared to the preceding interval. Sedimentation rates increased to ~0.72 cm/ka between 781 and 190.5 ka and then increased to ~1.2 cm/ka between 109.5 and 56 ka. The sedimentation rates increased substantially to ~9 cm/ka from 29 ka to present. The 29 ka and 56 ka ages are separated by 0.4 m stratigraphically suggesting an average sedimentation rate of ~1.5 cm/ka for this interval, but there is an erosional surface at 2.95 m so this is a minimum estimate. Sedimentologic and environmental magnetic evidence (discussed below) suggests that the large increase in sedimentation rate observed after 29 ka may have occurred immediately following the erosional event. In summary, the sedimentation rate increases progressively up the section, excluding the lowermost 2 m.

The dramatic increase in sedimentation rate associated with Pu1 (beginning 29 ka) and the presence of an A horizon (the modern soil) is particularly noteworthy in the context of the pedogenic model of Kemp and Zárate (2000). This unit does not appear to have been affected by the compound pedogenesis described by these authors, which means that loess deposition and subsequent soil formation occurred during one depositional/pedogenic cycle (i.e., one glacial/interglacial cycle). The fact that the loess from Pu1 was deposited during one glacial cycle makes the high sedimentation rates even more notable compared to the sedimentation rates of the other units. Although it is possible that a change in climate may have led to the increased sedimentation, it is also possible that sediment was eroded in the older pedologic units (e.g., Pu2–Pu4) during the multiple cycles of deposition and pedogensis. Kemp and Zárate (2000) favor diminished deposition over erosion in the sequences used for their model. Despite the uncertainties about loess accumulation and erosion that are specific to the Gorina Quarry sequence, their model provides a framework to explain the general absence of A horizons in our record.

5.2. Mineral-magnetic stratigraphy

It is apparent from the bulk magnetic coercivity (H_{cr} values ≤35 mT; Fig. 3) that the sediments of Gorina Quarry are dominated by low-coercivity ferrimagnetic minerals [e.g., (titano)magnetite and (titano)maghemite]. However, variations in the contribution of high-coercivity magnetic minerals (e.g., hematite and goethite) were observed throughout the section (*S*-ratio and HIRM; Fig. 3). These observations are consistent with those of Bidegain et al. (2007) who report that magnetite dominates the magnetic signature of both loess and paleosol units at Gorina Quarry. In addition, hematite was previously identified in sandy loess layers, whereas goethite was identified in carbonate-rich paleosols (Bidegain, 1998; Bidegain et al., 2007). Variations in the contributions of these minerals [*S*-ratio, HIRM, and $G/(G+H)$; Fig. 3] and the amount of ultrafine-grained magnetic minerals (<~25–30 nm), indicated by the frequency dependence of magnetic susceptibility (χ_{fd}%; Fig. 3), resulted in mass susceptibility (χ) values ranging from 0 to 3×10^{-6} m^3/kg (Fig. 3). The most pronounced mineralogical change occurred between 2.6 and 7 m where there was a decrease in the relative contribution of low-coercivity minerals (lower *S*-ratio values; Fig. 3). In addition, the relative amount of goethite to the total amount of high-coercivity minerals was much less variable and slightly lower from 0 to 7 m than it was below 7 m ($[G/(G+H)]$; Fig. 3).

In general, the magnetic grain size appears to be dominated by larger pseudo-single domain (PSD) grains (M_{rs}/M_s values between 0.1 and 0.2; Fig. 3) (Day et al., 1977; Thompson and Oldfield, 1986). The ARM/*K* and ARM/SIRM records are generally in-phase with M_{rs}/M_s while the SIRM/*K* record is not (Fig. 3). The SIRM/*K* record resembles all three concentration parameters (χ, SIRM, and ARM) and HIRM from 0 to 6.8 m (Pu1–Pu3; Fig. 3). From 6.8 to 9.1 m (Pu4), the SIRM/*K* does not resemble any of the other parameters, but from 9.1 m to the base of the section (Pu5–Pu6) it is in-phase with $ARM_{30\ mT}$/ARM (Fig. 3). In addition, the χ_{fd}% record is in-phase with the ARM/*K*, ARM/SIRM, and M_{rs}/M_s records for the entire section (Fig. 3).

The $ARM_{30\ mT}$/ARM record illustrates a phase opposition relative to ARM/*K* and ARM/SIRM (Fig. 3), suggesting finer magnetic grain sizes when the other parameters indicate coarsening. Although the ARM ratio contradicts the other grain size proxies, it is in-phase with the bulk grain size variations determined by Zárate et al. (2002); the highest $ARM_{30\ mT}$/ARM values (finest magnetic grains) corresponded to clayey silts while the lowest values (coarsest magnetic grains) corresponded to sandy silts.

These parameters and ratios indicate that coarse-grained minerals dominate the sediment of Gorina Quarry, however, there appears to be a wide range of grain sizes (e.g., high χ_{fd}% values indicative of ultrafine-grained minerals) present and mineralogical variations confound the parameters even further. This result is consistent with previous studies by Orgeira et al. (1998) who determined that MD magnetite was the dominant carrier of the magnetic signal and by Bidegain et al. (2005) who found a wide grain size range for the magnetite in their record. Magnetic variations were characterized with respect to the six pedologic units below.

5.2.1. Pedologic unit 1

This unit consists of the present surface soil and its parent loess (Zárate et al., 2009). There is an erosional surface at 2.95 m that

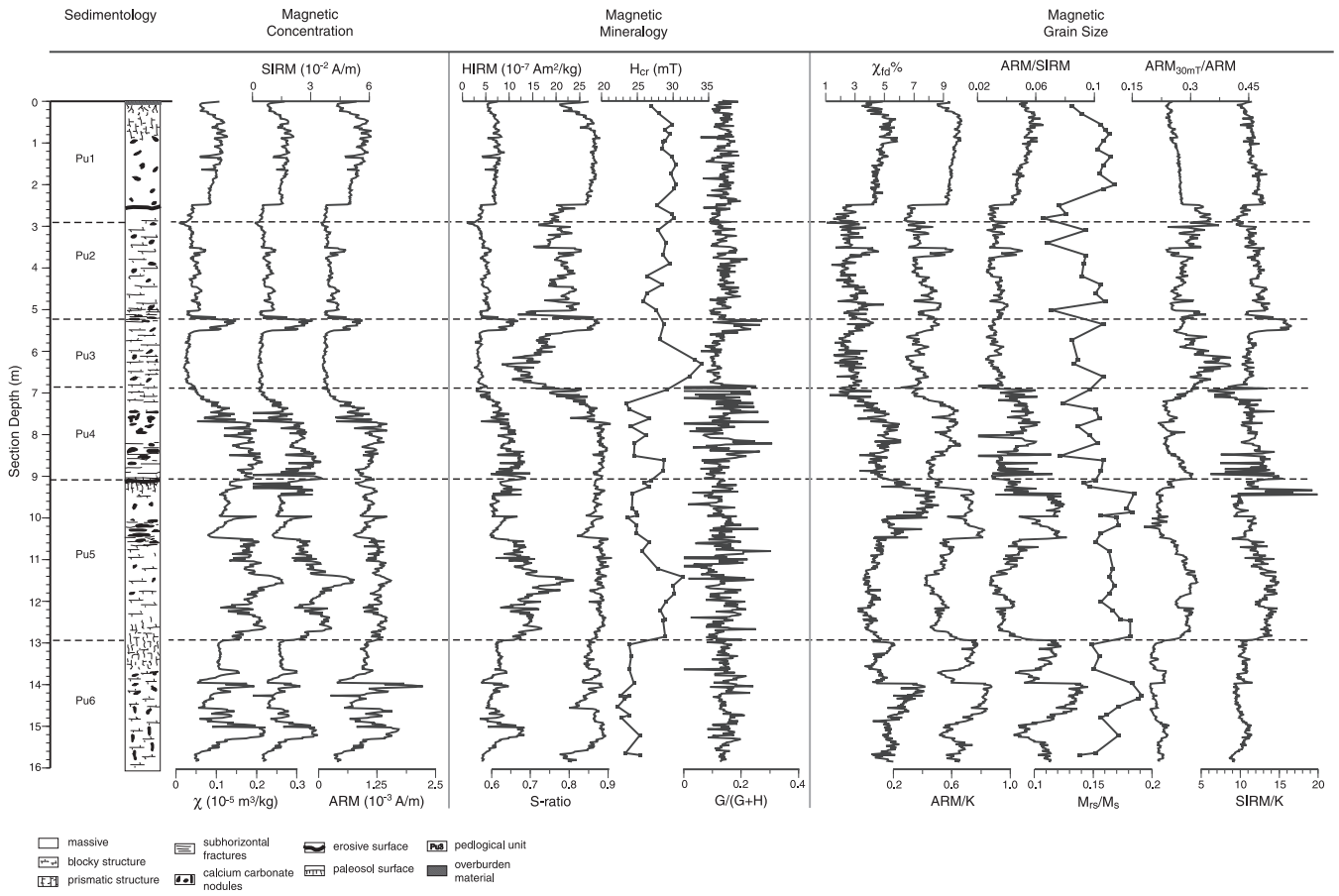

Fig. 3. Sedimentological log showing pedogenic units of Zárate et al. (2002). Environmental magnetic parameters used to characterize concentration, grain size, and mineralogical changes; parameters and ratios are discussed in Section 3 of the text.

marks a dramatic change in the environmental magnetic properties (Fig. 3). Previous studies interpreted the erosional surface as the boundary between the most recent pedologic unit (Pu1) and the previous pedologic unit (Pu2) (Zárate et al., 2002), but a recent reinterpretation by Zárate et al. (2009) indicates that the erosional surface was formed in the lower portion of Pu1. This reinterpretation is noteworthy because the magnetic properties below the erosional surface are more similar to those of Pu2 than those of Pu1 (Fig. 3). Above the erosional surface (the A–Ck2 horizons; 0–2.6 m), there is an abrupt increase in concentration parameters and an apparent fining in the grain size parameters with the exception of $ARM_{30\ mT}$/ARM (Fig. 3). In addition, there is an increase in the total amount of high-coercivity minerals coincident with a relative increase in low-coercivity minerals (higher HIRM and *S*-ratio values, respectively; Fig. 3). The χ_{fd}% increases slightly (approaching 6%) in the B horizons (0.4–1 m) but decreases in the A horizon (0–0.4 m). This decrease is associated with decreases in χ, *S*-ratio, and, to a lesser degree, HIRM. The Ck3 horizon (2.6–2.95 m) of this unit is markedly different than the Ck1 and Ck2 horizons (1–2.6 m) above in that it is characterized by low χ, *S*-ratio, and HIRM values.

5.2.2. Pedologic units 2 and 3

The Pu4–Pu3–Pu2 pedocomplex was differentiated by macroscale sedimentologic and possible diagnetic factors by Zárate et al. (2002). Based on our environmental magnetic properties, Pu2 and Pu3 are similar and are considered together, whereas Pu4 is distinctive and is considered separately. The Pu2 and Pu3 units are characterized by low χ, χ_{fd}%, and HIRM values, with the exception of high χ and HIRM values at the Pu2/Pu3 boundary (Fig. 3). The *S*-ratio and $ARM_{30\ mT}$/ARM are highly variable throughout these units. The Pu3 unit is characterized by lower *S*-ratio values and higher $ARM_{30\ mT}$/ARM values than the overlying Pu2 unit, but this transition begins in the upper portion of the Pu3 unit. These units consist entirely of B horizons that have varying amounts of carbonate content and have been exposed to periodic or permanent reduction (Zárate et al., 2002). In addition, these units consist of clayey silts, making them the finest grain size of the entire section (Zárate et al., 2002).

5.2.3. Pedologic unit 4

Unlike Pu3 and Pu2, this unit consists of A, B and C horizons. This unit is generally characterized by high χ, *S*-ratio, and HIRM values, but these values begin to decrease toward the low values of the overlying Pu3/Pu2 units in the A horizon (~6.8–7.4 m; Fig. 3). In general, the magnetic grain size parameters indicate the presence of finer grains. However, the $ARM_{30\ mT}$/ARM record is contradictory and suggests a coarsening of the magnetic grain size. The evidence for coarsening is consistent with an increase in bulk grain size to sandy silts (Zárate et al., 2002). The grain size parameters change in the C horizons (~8.5–9.1 m) of the lower portion of the unit. The χ_{fd}% values indicate that there is little or no production of ultrafine-grained magnetic minerals in the C horizons, which is consistent with the typical unaltered nature expected in parent material.

5.2.4. Pedologic unit 5

The upper boundary of this unit is truncated by an erosional surface at the top of a Bt horizon (9.1 m; Zárate et al., 2002). The unit grades into a BC and then a BCk horizon within the top ~1.5 m

(9.1–10.5 m) at which point there are abundant carbonate nodules (Fig. 3). The upper 1.5 m of this unit are characterized by intermediate χ and HIRM values, and the highest χ_{fd}% values (>8%) of the section. The remainder of the unit is a BCk horizon (10.5–12.9 m) and is characterized by higher magnetic concentrations and intermediate χ_{fd}% values. The $ARM_{30\ mT}$/ARM record is consistent with bulk grain size variations in the upper 1.5 m of the unit and indicates coarser magnetic grains in a sandy silt matrix (Zárate et al., 2002), which is contradictory to the other magnetic grain size parameters (Fig. 3).

5.2.5. Pedologic unit 6

This unit is similar to Pu5 in that it contains a surface Bt horizon with an underlying BCk horizon(s). The Bt horizon (12.9–13.8 m) is characterized by intermediate χ, χ_{fd}%, and HIRM values (Fig. 3). The out-of-phase magnetic grain size relationship persists throughout this unit such that low $ARM_{30\ mT}$/ARM values indicate generally coarser magnetic grains while other parameters suggest finer magnetic grain sizes. There is an increase in the ultrafine-grained component (χ_{fd}%) at ~13.8 m, which is coincident with an increase in the abundance of carbonate nodules (Fig. 3). The BCk interval (13.8–16 m) is characterized by variable (intermediate to high) χ, *S*-ratio, and HIRM values.

6. Discussion

6.1. Magnetic grain size

Magnetic grains size records are an important paleoenvironmental proxy that have the potential to provide insight into depositional and/or postdepositional processes. The magnetic grain size parameters used in this study are convenient, qualitative measures but must be considered in the context of magnetic mineralogical and concentration changes. This is evident in the apparent discrepancy between the $ARM_{30\ mT}$/ARM ratio and the other well-established grain size proxies (M_{rs}/M_s, ARM/*K*, ARM/SIRM, and SIRM/*K*). These interparametric ratios can be confounded by mineralogical variations and contributions by nonremanence-carrying grain sizes (<30 nm), much like those observed in the Gorina Quarry section (Fig. 3). The two parameters that are least affected by mineralogical variations are $ARM_{30\ mT}$/ARM and χ_{fd}%. The ARM ratio is sensitive to fine-grained ferrimagnetic minerals (Dunlop and Özdemir, 1997) while χ_{fd}% reflects the relative contribution of superparamagnetic material (<~25–30 nm; Dunlop and Özdemir, 1997).

Typical χ_{fd}% values associated with the formation of ultrafine-grained minerals during pedogenesis are ~5–8% (Liu et al., 2007 and references therein). Based on the C horizons preserved at Gorina Quarry, typical non-pedogenic χ_{fd}% values range from 4 to 5% (Pu1 and Pu4; Fig. 3). In addition, the lowest χ_{fd}% values at Gorina Quarry (<4%, but typically ~2%) appear to be associated with reducing conditions in poorly drained soil horizons (Pu2 and Pu3; Fig. 3) (Zárate et al., 2002). This is consistent with the findings of Bidegain et al. (2005) who found similarly low χ_{fd}% values from other gleyed soils in the region. Reducing conditions, commonly associated with soil gleying, result in the destruction of fine-grained ferrimagnetic minerals (Maher, 1986; Liu et al., 2001; Bidegain et al., 2005). Since χ_{fd}% appears to be an indicator of postdepositional formation and/or destruction of ultrafine-grained magnetic minerals, it is likely that M_{rs}/M_s, ARM/*K*, and ARM/SIRM are also indicators of postdepositional grain size variations (in a larger size range) since those records respond in-phase with χ_{fd}%. Conversely, the $ARM_{30\ mT}$/ARM values respond in the opposite manner to the other grain size parameters but more closely match the bulk grain size variations determined by Zárate et al. (2002). This relationship suggests that the ARM ratio is an indicator of depositional changes in fine-grained ferrimagnetic minerals. This result is consistent with the findings of Blanchet et al. (2007) who found that the ARM ratio demonstrated a linear relationship to the clay/silt ratio (from a terrigenous source) while contradicting the other magnetic grain size proxies (e.g., ARM/*K* and SIRM/*K*).

6.2. Wind patterns

The relationship outlined above suggests that $ARM_{30\ mT}$/ARM may be considered as a continuous analog for variations in bulk grain size changes in the Gorina Quarry section. In general, there are systematic grain size changes (bulk and magnetic) at pedologic unit boundaries (Fig. 3) and, based on our age model, it is apparent that large amplitude variations in $ARM_{30\ mT}$/ARM occur on a 500–600-ka timescale (Fig. 4a), which equates to a 1–1.2 Ma cycle. Berger and Loutre (1991) demonstrated that a 1.19-Ma period can be generated by the 41.09-ka and 39.71-ka periods of obliquity for the last 10 Ma. A comparison of our $ARM_{30\ mT}$/ARM record to the obliquity signal filtered at 1.2-Ma demonstrated a good agreement between the records over the 0.4–1.94 Ma time period (Fig. 4a). The relationship indicates that finer magnetic grain sizes (higher $ARM_{30\ mT}$/ARM values) occurred during periods of high obliquity amplitude. Oxygen isotope records indicate that glaciations are stronger during periods of high amplitude obliquity (e.g., Lisiecki and Raymo, 2005), which means that magnetic (and bulk) grain size in our record was finest during strong glacial intervals. At face value, this appears to be counterintuitive since it is generally accepted that glacial periods are associated with stronger winds and stronger winds can carry coarser material longer distances (Pye, 1987, p. 51). We propose a mechanism to explain this grain size phenomenon that involves a northward displacement of the continental high-pressure cell during glacial periods.

The present configuration of atmospheric pressure at sea level during austral winter has a small high-pressure cell centered at 34°S and 64°W (Fig. 5a; Schwerdtfeger, 1976). Marine records from the southeast Atlantic and southeast Pacific indicate that the Antarctic Circumpolar Current is displaced northwards during glacial periods (e.g., Becquey and Gersonde, 2002; Lamy et al., 2004) and as a result, atmospheric circulation patterns are affected in the same manner (e.g., Heusser, 1991). Based on these studies, it is likely that the high-pressure cell located over central South America is displaced northward during glacial intervals. We propose a scenario in which the extent of this northward displacement is related to the strength of glaciations, such that stronger glaciations result in a more northerly displacement (Fig. 5b and c). It is possible that this differential displacement of the high-pressure cell is a factor controlling the magnetic grain size in the sediments deposited at Gorina Quarry.

This model provides a mechanism to alter wind patterns in subtropical South America over glacial/interglacial timescales, but it is necessary to consider how these positional changes translate to changes in the magnetic grain size of the loess deposited at our study location. Like bulk grain size, changes in magnetic grain size are controlled by the type of source sediment(s), proximity to the source(s), and wind strength and/or direction. Zárate and Blasi (1993) suggest that loess deposited in southern Buenos Aires was derived from the lower reaches of the Rio Colorado and Negro, which both derive their sediment from Patagonia and the south central Andes. Of these two similar source regions, the Rio Colorado and Negro source region is closer to our study location. In our model, the high-pressure cell is located closer to the Rio Colorado and Negro source region during weaker glacial periods (Fig. 5b) than it is during stronger glacial periods (Fig. 5c). Winds from the high-pressure cell are likely to carry sediment from the Rio

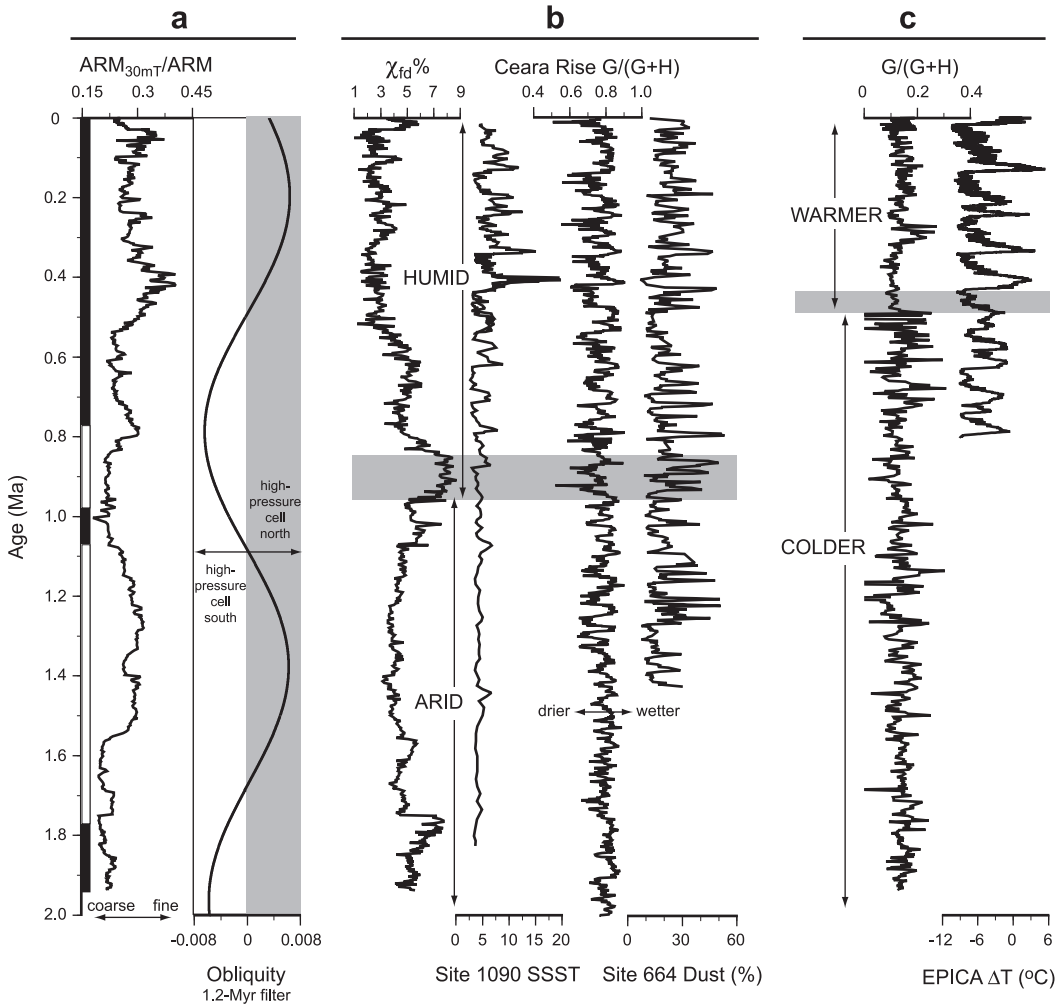

Fig. 4. (a) $ARM_{30\ mT}$/ARM compared to the obliquity signal filtered at 1.2-Myr (Laskar et al., 2004). Prior to ~400 ka magnetic grain size increases during periods of low obliquity amplitude. The differential northward displacement of the wind system changes the sediment source proximity and/or wind strength (discussed in Section 6.2). (b) χ_{fd}% compared to the summer sea surface temperature (SSST) record from Site 1090 in the southeast Atlantic Ocean (Becquey and Gersonde, 2002, 2003), the $G/(G+H)$ ratio from Ceara Rise (Harris and Mix, 2002), and the terrigenous input (dust) record from Site 664 (deMenocal, 1995). The increase in ultrafine-grained magnetic minerals around 0.96 Ma coupled with sedimentologic and environmental magnetic evidence for gleying beginning at ~0.5 Ma suggests an increase in moisture. A southward displacement of the southeast trade winds shifted moisture transport from tropical South America to subtropical South America. The increase in dust at Site 664 suggests a possible northern hemisphere mechanism (discussed in Section 6.3). (c) The $G/(G+H)$ record from Gorina Quarry compared to the temperature reconstruction from the EPICA Dome C ice core (Jouzel et al., 2007). Our interpretation of increased temperature [lower $G/(G+H)$ values] beginning around 450 ka is consistent with increased interglacial temperatures observed in the EPICA record.

Colorado and Negro source region during weaker glacial intervals and from Patagonia and the south central Andes source region during stronger glacial intervals. Since the Rio Colorado and Negro source region is closer to our study area it is likely that coarser magnetic (and bulk) grain sizes could be transported to our site by the wind whereas they are less likely to be transported from Patagonia and the south central Andes (e.g., Pye, 1987, p. 51).

Despite the evidence for changes in the source region and the proximity to our study location, it is not possible to exclude changes in wind strength as a mechanism to explain the magnetic grain size variations in our record. In addition, it is important to note that the duration of our record (~1.9 Myrs) is not long enough to definitively identify and characterize long-term (>1 Myr) orbital variations. The synchroneity of our magnetic grain size record and the 1.2-Myr modulated obliquity signal (Fig. 4) was the basis for our comparison and is presented here as a possible mechanism with the understanding of its limitations. It is evident that further work is needed to establish the validity of our model and to better understand the temporal variations in aeolian deposition as it relates to sediment sources and wind strength/direction.

6.3. Moisture

Several studies have used χ_{fd}% as an indicator of changes in the superparamagnetic grain size fraction and have related those changes to pedogenesis and its relationship to rainfall and paleomonsoon intensity (e.g., Maher et al., 1994, 2002; Maher and Thompson, 1995; Chen et al., 1999; Deng et al., 2005). Typically, χ_{fd}% values between ~5 and 8% indicate the presence of ultrafine-grained minerals formed during pedogenesis (Liu et al., 2007 and references therein). Based on our proposed age model, there are three intervals that reach and/or exceed χ_{fd}% values of 5% in the Gorina section: the late Pliocene and very early Pleistocene (1.75–1.94 Ma), the mid-Pleistocene (0.6–1.07 Ma), and the very late Pleistocene and Holocene (~30 ka – present) (Fig. 4b). The χ_{fd}% values showed a decreasing trend from their peak values at 0.96 Ma until 0.6 Ma, at which time they remained low (~2%) until 30 ka. Bidegain et al. (2005) indicated that χ_{fd}% values in this range are typical for gleyed sediments. In view of sedimentologic evidence for gleying and overall finer bulk grain size in this interval (Zárate et al., 2002), it is likely that the decrease in the ultrafine-grained fraction

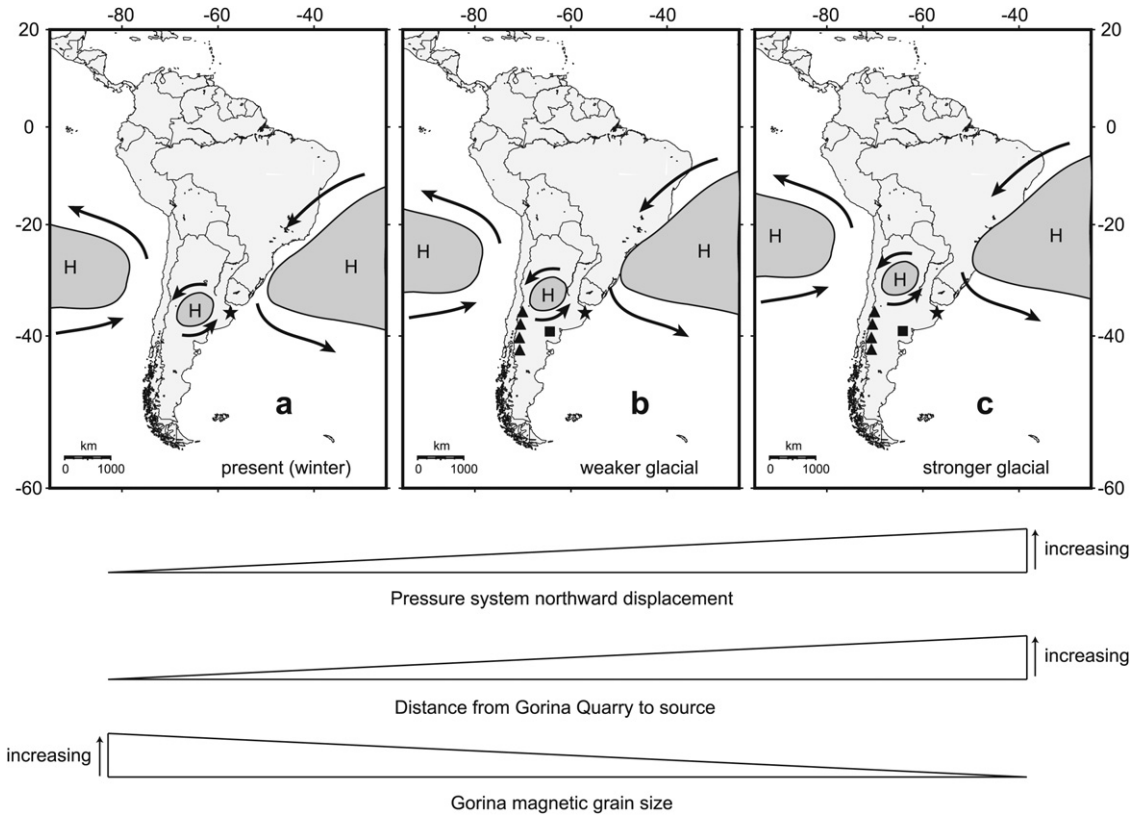

Fig. 5. Schematic representation of the location of atmospheric pressure cells and associated wind patterns during interglacial periods (a), weaker glacial periods (b), and stronger glacial periods (c). The increased northward displacement during stronger glacial periods increases the distance between Gorina Quarry and the source region, resulting in finer magnetic grain sizes. The black square and the black triangles in (b) and (c) represent the location of the Rio Colorado/Negro source region and the Patagonia/Andes source region (Smith et al., 2003), respectively. The present configuration (a) is taken from Schwerdtfeger (1976). The star indicates the location of Gorina Quarry.

resulted from intermittent reducing conditions associated with waterlogged soils (Maher, 1986; Liu et al., 2001; Bidegain et al., 2005).

Here we focus on the notable increase in χ_{fd}% that occurs around 0.96 Ma (Fig. 4b) and the apparent increased humidity from that point on. The timing of this increase is similar to that of the mid-Pleistocene transition (MPT) which is characterized by a change from a world dominated by the 41 ka obliquity cycle to the 100 ka eccentricity cycle around 0.9 Ma (Raymo et al., 1989; Ruddiman et al., 1989). Much of the work relating to the MPT has come from marine isotopic studies (e.g., Raymo et al., 1997; Huybers, 2007), but there are limited studies relating oceanic changes associated with the MPT to a terrestrial environment. Here we attempt to make that connection and provide plausible mechanisms to explain the changes observed in our record.

Several studies indicate that the transport of moisture to tropical South America is influenced by the position and strength of the South Atlantic Anticyclone (SAA) and the Pacific Anticyclone (PA) (e.g., Villagrán, 1993; Cruz et al., 2006). Based on these studies, we compared our χ_{fd}% record to the summer sea surface temperature (SSST) record from the South Atlantic sector of the Southern Ocean of Becquey and Gersonde (2002, 2003; Fig. 4b). Their SSST reconstructions along a north–south transect across the Antarctic Circumpolar Current (ACC) from ODP Leg 177 showed the migration of the oceanic frontal systems (the Subtropical Front, the Subantarctic Front and the Polar Front) throughout the Pleistocene and Holocene (Becquey and Gersonde, 2002, 2003). Their results for the early to mid-Pleistocene (1.83–0.87 Ma) indicated generally low SSST values (3–5 °C) with minor changes (~2 °C) between glacial and interglacial periods, suggesting a northward shift of the Polar Front Zone (PFZ) by about 7° latitude relative to its present position (Becquey and Gersonde, 2002). Based on our record, the driest conditions in central eastern Argentina occurred from ~0.96 to 1.93 Ma, when SSSTs were lowest and least variable between glacial and interglacial stages (Fig. 4b). We attribute the relative aridity of central eastern Argentina during this time period to the diminished strength and northward displacement of the SAA associated with colder SSSTs, and a 7° northward shift of the PFZ. In this state, the diminished strength of the SAA carried less moisture to tropical and subtropical South America (Fig. 6a).

During the mid- to late Pleistocene and Holocene, SSSTs in the Southern Ocean increased and became more variable (Fig. 4b) (Becquey and Gersonde, 2003). Although glacial SSSTs increased slightly, interglacial SSSTs increased in two steps. The first increase occurred around 0.87 Ma and the second, more dramatic increase occurred at 0.43 Ma (Fig. 4b). With these warmer interglacial SSSTs, the PFZ shifted southward toward its present location, as is likely to happen with the SAA (Fig. 6b). In this configuration, the southern trade winds were in a more southerly location allowing for more moisture to be carried to subtropical South America.

To support our model, we compared our record to the $G/(G+H)$ of ODP Site 926, the Ceara Rise (Harris and Mix, 1999, 2002). The sediments from this location reflect changes in continental erosion relating to climatic and tectonic mechanisms, and the $G/(G+H)$ record is used as a proxy for precipitation in the Amazon lowlands or the pre-Amazon drainage areas (Harris and Mix, 1999, 2002). They related the $G/(G+H)$ ratio to precipitation such that high values indicated increased precipitation in the terrigenous lowlands. The $G/(G+H)$ record from Ceara Rise shows a decrease in ratio values beginning around 0.95 Ma (Fig. 4b) indicating that

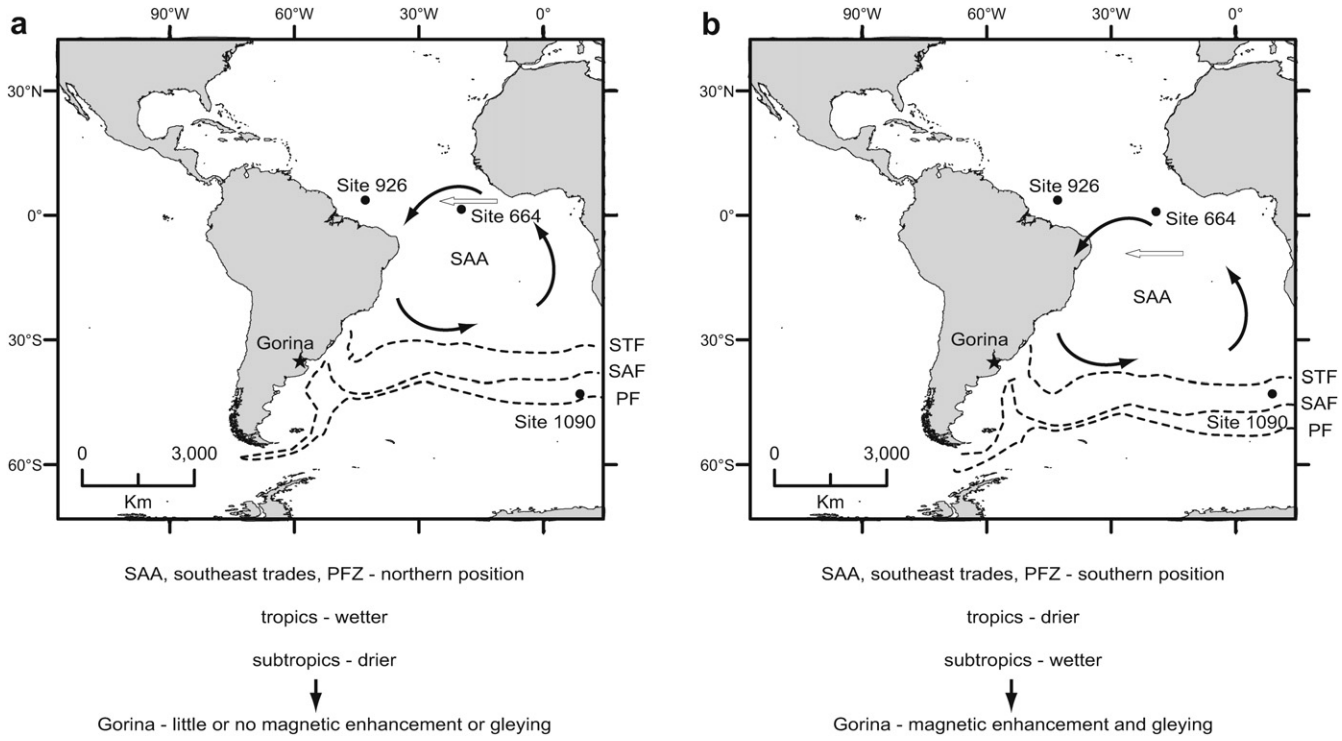

Fig. 6. Position of the South Atlantic Anticyclone (SAA) for (a) the early to mid-Pleistocene (0.96–1.93 Ma) and (b) the mid- to late Pleistocene and Holocene (0.96 Ma-present). The present position of the SAA is taken from Peterson and Stramma (1991). The white arrow in each diagram indicates the relative position of the southern trade winds (and associated moisture transport direction). The dashed lines are a schematic representation of the frontal zones of the Antarctic Circumpolar Current (from Peterson and Stramma, 1991); Subtropical Front (STF), Subantarctic Front (SAF), and the Polar Front (PF). The positions of these hydrographic boundaries are shown relative to the location of the SSST reconstruction of ODP Site 1090, the $G/(G+H)$ record of Ceara Rise (Site 926), and the dust record of Site 664. The star indicates the location of Gorina Quarry.

precipitation decreased in the Amazon lowlands after the mid-Pleistocene. This result is consistent with the redirection of moisture from tropical South America to subtropical South America associated with the southward displacement of the SAA and southern trades proposed in our model.

Our model provides a southern hemisphere mechanism to explain changes in moisture to tropical and subtropical South America around 1 Ma, but it is possible that the intensification of northern hemisphere glaciation around that time (Ruddiman et al., 1989; Raymo, 1994) may have altered the position and strength of the trade winds. Marine records of African climate variability show an increase in the concentration of aeolian sediment around 1 Ma (deMenocal, 1995). Model simulations show that cold North Atlantic sea surface temperatures (SSTs) strengthen the subtropical Atlantic high-pressure cell resulting in strengthened northeast trade winds (deMenocal, 1995). The combination of cold SSTs and strengthened winds led to increased African aridity and the resulting increase in aeolian material in the marine records. Ruddiman and Janecek (1989) suggested that increased dust flux to equatorial Atlantic Site 664 (ODP Leg 108) may have been the result of a more southerly position of the Intertropical Convergence Zone (ITCZ) over Africa. A comparison of the amount of terrigenous detritus from Site 664 (deMenocal, 1995) to our χ_{fd}% record (Fig. 4b) indicates an initial increase in dust just prior to 1.2 Ma and a second increase just prior to 0.9 Ma, which is similar in timing to the increase in moisture from our record (increased χ_{fd}% at 0.96 Ma). If the ITCZ was in a more southern position beginning around that time, the southeast trades would have been in a more southerly position as well, providing the same change in moisture transport suggested in our model.

Having presented two scenarios to explain the changes observed in our record, it seems increasingly likely that the position and/or strength of the southeast trade winds changed around 1 Ma, similar in timing to the MPT. At this point it is unclear whether one scenario is the dominant mechanism controlling moisture transport to subtropical South America or if both processes are involved.

6.4. Temperature

Schwertmann (1988) and Kämpf and Schwertmann (1983) indicated that the formation of hematite (αFe_2O_3) and goethite (αFeOOH) is related, at least in part, to moisture and temperature in such a way that the relative amount of goethite increases exponentially as excess moisture increases, whereas the amount of hematite increases with increased air temperature. Our environmental magnetic record indicates a decrease in the $G/(G+H)$ ratio around 500 ka (Fig. 4c) that can be attributed to several factors including increasing air temperature, decreasing moisture, decreasing soil organic matter, or increasing pH (Kämpf and Schwertmann, 1983). Although it is difficult to elucidate these factors on magnetic proxies alone, we attempted to exclude several factors based on other environmental magnetic properties and sedimentologic evidence. Based on our previous discussion about moisture, it does not appear that moisture decreased during this time interval. Since soil moisture is intimately linked to vegetation, it is also likely that soil organic matter did not decrease. In addition, the presence of calcium carbonate nodules throughout the section suggests that there was no appreciable change in soil pH. Therefore, it is likely that this decrease in $G/(G+H)$ is related to an increase in temperature. Based on these assumptions, our conclusions about increasing temperature are consistent with the high-resolution temperature reconstruction obtained from the EPICA Dome C ice core (Jouzel et al., 2007) that showed an increase in interglacial temperatures by as much as 6 °C (relative to the average

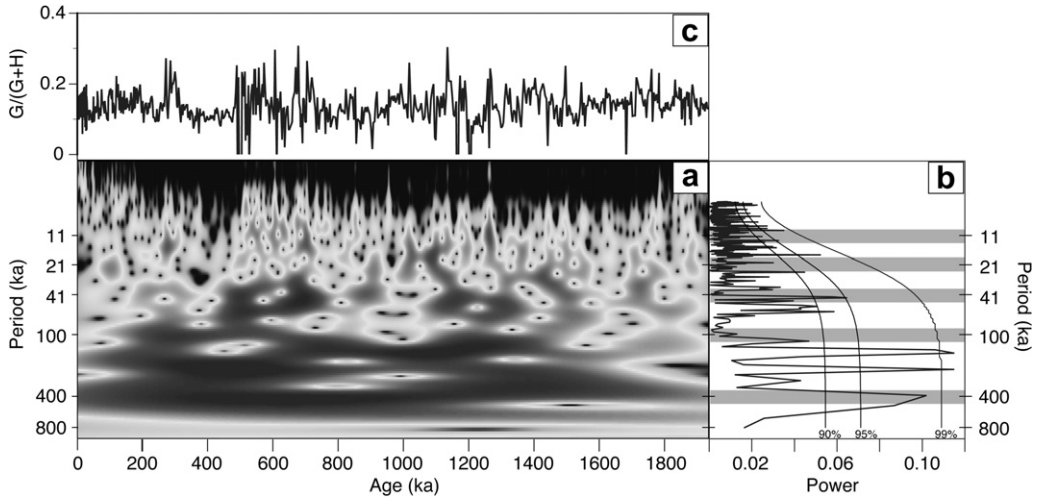

Fig. 7. Wavelet (a) and spectral (b) analysis of $G/(G+H)$ from Gorina Quarry. Several cycles are identified (41, 125, 250, 400 ka), however, their presence is variable, as indicated by the wavelet analysis. The shaded horizontal bars in (b) represent the typical Milankovitch orbital periodicities. (c) $G/(G+H)$ record versus age. Wavelet software was provided by C. Torrence and G. Compo, and is available at URL: http://atoc.colorado.edu/research/wavelets/. Spectral analysis was performed using REDFIT 3.5 (Schulz and Mudelsee, 2002).

temperature of the last 1000 years) since the mid-Brunhes Event (~450 ka; Jouzel et al., 2007).

6.5. Pedogenesis and insolation

The sedimentology and micromorphology of the Gorina Quarry section (Zárate et al., 2002) indicate that, with the exception of the surface soil (Pu1), the sequence has a complex pedosedimentary history of welding that inhibits differentiation of discrete paleosol units. The pedologic units identified by Zárate et al. (2002), and discussed in this study, are based more on grain size variations than on macro or micromorphological evidence of pedosedimentary processes. Kemp and Zárate (2000) described a pedosedimentary model for Pliocene deposits in the southern Pampas of Argentina that involved continuous pedogenesis during periods of deposition, resulting in continual alteration of loess and previous soil horizons. It is likely that this model is an appropriate analog for the sequence at Gorina Quarry (Zárate et al., 2002). Despite the complex depositional and pedogenic history of the Pliocene deposits, Kemp and Zárate (2000) identified cyclic behavior in sedimentation and pedogenesis. They determined that periods of reduced sedimentation and stable landscapes resulted in clearly defined eluvial and illuvial horizons while periods of increased sedimentation resulted in welding of new pedologic features on existing soils. If the same pedosedimentary model is a reasonable analog for sedimentation and pedogensis at Gorina Quarry, it is reasonable to expect at least some degree of depositional and/or pedogenic cycles to be preserved in the sediment record of Gorina Quarry.

It is apparent from variations in magnetic grain size and bulk grain size that the Gorina Quarry sequence records long-wavelength (~1.2 Ma; Fig. 4a) changes in deposition relating to changes in wind patterns and source regions. In addition, spectral and wavelet analysis of the $G/(G+H)$ ratio indicates cyclic behavior relating to postdepositional processes (Fig. 7). The periodogram shows peaks in the mid and low frequency range (~41, 125, 250, and 400 ka periods) (Fig. 7b) and the wavelet shows the variable

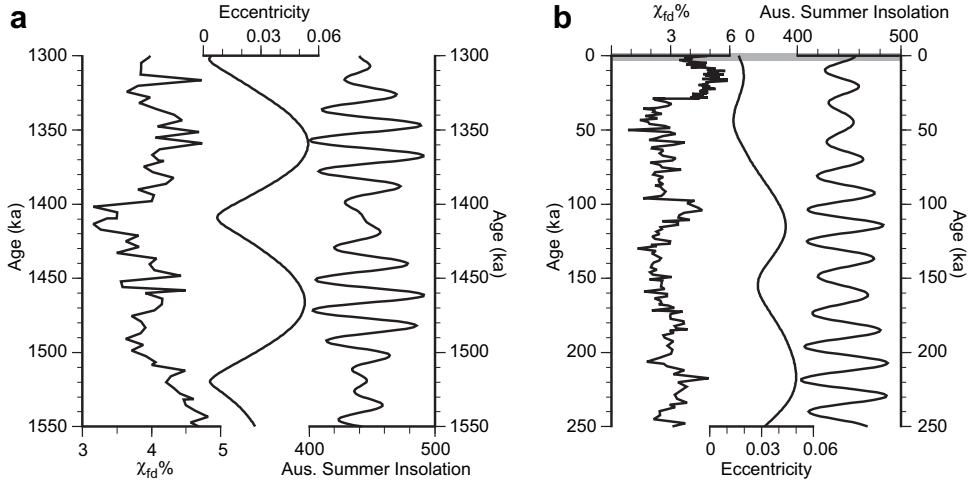

Fig. 8. (a) The χ_{fd}% record from 1.3 to 1.55 Ma compared to eccentricity and austral summer insolation from 30°S (Laskar et al., 2004). There is a significant correlation between χ_{fd}% and eccentricity (p-value = 0.0273). Preservation of ultrafine-grained ferrimagnetic minerals (high χ_{fd}% values) corresponds to high eccentricity and highest insolation. (b) χ_{fd}% from 0 to 250 ka compared to eccentricity and austral summer insolation from 30°S (Laskar et al., 2004) indicating the preservation of ultrafine-grained ferrimagnetic minerals during periods of high eccentricity and insolation (p-value = 0.0239). The shaded horizontal bar in the top of (b) corresponds to the A horizon of the present surface soil (Zárate et al., 2002). The ultrafine-grained minerals are depleted in the A horizon which corresponds to relatively low insolation and low eccentricity.

Table 1
General characteristics of Argentine loess/paleosol record compared to Alaskan and Chinese.

Location	Argentina (Gorina Quarry)	Alaska	China
Sedimentation rates	0.38–1.2 cm/ka (excluding Pu1 9 cm/ka)	~6.5 cm/ka (Begét et al., 1990)	~6–18 cm/ka (Lu and Sun, 2000)
Discrete paleosols	Rare (only two A horizons preserved)	Prominent	Prominent
Interglacials	Pedogenic depletion of ferrimagnetic minerals; lower magnetic concentration	Pedogenic depletion of ferrimagnetic minerals; lower magnetic concentration	Pedogenic enhancement of magnetic minerals; higher magnetic concentration
Glacials	Deposition of ferri and antiferromagnetic magnetic minerals; coarser grained during weaker glacials; higher magnetic concentration	Deposition of ferrimagnetic minerals; coarser grains during stronger glacials; higher magnetic concentration	Deposition of ferri and antiferromagnetic magnetic minerals; coarser grains during glacials; lower magnetic concentration
Orbital periods	Present sporadically	Present prominently	Present prominently

presence of these periods throughout the section (Fig. 7a). Although these periods are similar to Milankovitch-type orbital periods, the uncertainties associated with the broad peaks and intermittent presences suggest that other mechanisms (e.g., regional climate) play an important role in postdepositional processes. A rigorous characterization of the spectral properties of the Gorina Quarry section is beyond the goals of this paper. The spectral and wavelet analysis was intended to demonstrate that, despite the pedosedimentary complexity of the section, the environmental magnetic properties record cyclic behavior like the Pliocene sections of Kemp and Zárate (2000).

Although the spectral record from Gorina Quarry is complex and variable, there are portions of the record that suggest relationships to eccentricity and insolation (Fig. 8). Here we examine the χ_{fd}% record from two time intervals and discuss notable similarities when compared to the eccentricity record and austral summer insolation. The first interval spans the time period 1.3–1.55 Ma and covers the lower portion of Pu5. The χ_{fd}% records a relatively higher amount of ultrafine magnetic minerals (higher χ_{fd}% values) during peak eccentricity and higher amplitude insolation (Fig. 8a). There appears to be a significant correlation between eccentricity and the amount of ultrafine-grained ferrimagnetic minerals (p-value = 0.0273). Considering the relationship between χ_{fd}% and precipitation (e.g., Maher et al., 1994, 2002; Maher and Thompson, 1995; Chen et al., 1999; Deng et al., 2005) it is likely that precipitation increased during intervals of higher amplitude insolation. However, the χ_{fd}% values are lower than those resulting from pedogenic enhancement (>5%; Liu et al., 2007). It is likely that our data record changes in the preservation of ultrafine-grained magnetic minerals during pedogenesis versus their formation. This interpretation would be similar to that invoked for the Alaskan and Siberian loess/paleosol records that display pedogenic destruction of ferrimagnetic minerals (Begét and Hawkins, 1989; Liu et al., 2001, 2008). In these records, the destruction of ferrimagnetic minerals was caused by increased temperature and moisture that increased the reducing potential of the soils (Liu et al., 2008). If the same process occurred in this interval at our location, then it would appear that the pedogenic destruction of the ferrimagnetic minerals occurred during periods of lower eccentricity and lower insolation amplitude, which would imply that these periods were wetter and/or warmer. Since it seems unlikely that it would be warmer during periods of low insolation amplitude, it is likely that soil moisture was higher during these times due to either increased precipitation or lower evaporation.

A similar relationship exists among χ_{fd}%, eccentricity and insolation for the period 30–250 ka (p-value = 0.0239) (Fig. 8b). This interval spans all of Pu2 and the upper portion of Pu3 and appears to have been subjected to a degree of gleying. The reducing conditions associated with gleyed soils are likely to diminish the amount of ferrimagnetic minerals, which is reflected by the lowest S-ratio values of the entire sequence (Fig. 3). Although this interval was deposited/altered during a different climatic regime than the older interval discussed above, it appears as though eccentricity and insolation played a similar role in the preservation of ferrimagnetic minerals.

In addition, the A horizon of the surface soil (Pu1) appears to be diminished in ferrimagnetic minerals compared to the B and C (loess) horizons (Fig. 3). The decrease in ferrimagnetic minerals in the A horizon corresponds to a decrease in eccentricity and relatively low insolation amplitude (shaded region in Fig. 8b).

The evidence from these intervals suggests insolation is an important factor in the preservation of ferrimagnetic minerals during pedogenesis. Although the relationship does not persist throughout the entire sequence (e.g., the interval between 0.8 and 1.1 Ma), it seems as though the magnetic record of pedogensis from the Gorina Quarry sequence is more similar to the Alaskan loess sequences than the Chinese loess sequences. A comparison of the general characteristics of the Gorina Quarry loess/paleosol sequence to those of the Alaskan and Chinese loess/paleosol sequences are outlined in Table 1. Although there are more similarities between our record and the Alaskan sequences compared to the Chinese sequences, it is worth noting the profound difference in sedimentation rates (Table 1). The average sedimentation rates from Alaska and China are at least 6 times higher (Begét et al., 1990; Lu and Sun, 2000) than those in our record. Whether the low sedimentation rates in our record are the result of diminished deposition or erosion, it appears as though they are a limiting factor in the preservation and/or recording of climate cycles. This point is accentuated in Pu1, which has an average sedimentation rate of 9 cm/kyr (within the range of the Alaskan and Chinese sequences) and demonstrates the well-developed soil horizons that define glacial/interglacial boundaries in both China and Alaska.

7. Conclusions

We characterized the environmental magnetic record for the last ~1.9 Ma from the central eastern Pampas of Buenos Aires, Argentina. The ~16 m section resulted from the accretion of coarse to fine grained aeolian material and consists of six pedologic units. Although the pedologic units are distinguished by bulk sedimentological changes and not by macro or micromorphological pedogenic indicators, there are systematic changes in the environmental magnetic properties associated with each pedologic unit. Understanding these changes in the context of depositional and/or postdepositional processes provide some insight into potential mechanisms relating to regional and global climate change.

Using a paleomagnetic reversal stratigraphy and optically stimulated luminescence ages, we constrained the timing of several sedimentological and environmental magnetic changes and related them to major climate transitions with plausible mechanisms:

- Long-wavelength (~1.2 Ma) cycles in ferrimagnetic mineral grain size and bulk grain size were attributed to a differential

northward displacement of the high-pressure cell and the associated winds.
- An increase in the amount of ultrafine-grained magnetic minerals coupled with sedimentologic evidence suggests an increase in moisture at 0.96 Ma. This change in moisture availability was linked to a southward displacement of the trade winds and the associated moisture at the mid-Pleistocene transition, caused by increased sea surface temperatures in the South Atlantic or by a decrease in North Atlantic sea surface temperatures.
- A relative decrease in the amount of goethite over hematite suggested that temperature increased at our study location around 500 ka, which is similar in timing to the temperature increase observed in the EPICA Dome C ice core record following the mid-Brunhes Event (~450 ka).
- Although the spectral record is inconsistent, it is evident that orbital and non-orbital cycles are recorded (if only intermittently) in the environmental magnetic record from Gorina Quarry.
- Portions of the magnetic record demonstrated a relationship to eccentricity and insolation such that ultrafine-grained ferrimagnetic minerals were destroyed during periods of low insolation. This evidence suggests that the magnetic model for pedogensis is more similar to that of the Alaskan loess sequences than the Chinese loess sequences.

This study presented one of the longest and most continuous environmental magnetic records from the loess/loessoid deposits of Argentina. Our models and mechanisms are proposed to explain the environmental magnetic and sedimentological variations observed at Gorina Quarry; however, it is evident that further work is required to test them. Despite the inherent uncertainties, it is clear that the environmental magnetic record from the loess and paleosol deposits in the central eastern Pampas of Buenos Aires records major changes in deposition and soil formation.

Acknowledgements

This research was supported by NSF Grant EAR-0001047 and partial support for C. Heil was from a NASA/RI Space Grant Fellowship. We thank James King, Dane Sheldon, and Caroline Greene Hunt for their help in sample preparation. We'd also like to thank T. Evans and Q. Liu for their thoughtful reviews and comments of this paper and an earlier version.

Appendix. Supplementary data

Supplementary data associated with this article can be found in the online version, at doi:10.1016/j.quascirev.2010.06.024.

References

Becquey, S., Gersonde, R., 2002. Past hydrographic and climatic changes in the Subantarctic Zone of the South Atlantic – the Pleistocene record from ODP site 1090. Palaeogeography, Palaeoclimatology, Palaeoecology 182, 221–239.
Becquey, S., Gersonde, R., 2003. A 0.55-Ma paleotemperature record from the Subantarctic zone: implications for Antarctic Circumpolar Current development. Paleoceanography 18 (1), 1014. doi:10.1029/2000PA000576.
Begét, J.E., Stone, D.B., Hawkins, D.B., 1990. Paleoclimatic forcing of magnetic susceptibility variations in Alaskan loess during the late Quaternary. Geology 18, 40–43.
Begét, J.E., Hawkins, D.B., 1989. Influence of orbital parameters on Pleistocene loess deposition in central Alaska. Nature 337, 151–153.
Berger, A., Loutre, M.F., 1991. Insolation values for the climate of the last 10 million years. Quaternary Science Reviews 10, 297–317.
Bidegain, J.C., 1998. New evidence of the Brunhes/Matuyama polarity boundary in the Hernández-Gorina quarries, northwest of the city of La Plata, Buenos Aires province, Argentina. Quaternary of South America and Antarctic Peninsula 11, 207–228.
Bidegain, J.C., Evans, M.E., van Velzen, A.J., 2005. A magnetoclimatological investigation of Pampean loess, Argentina. Geophysical Journal International 160, 55–62.
Bidegain, J.C., van Velzen, A.J., Rico, Y., 2007. The Brunhes/Matuyama boundary and magnetic parameters related to climatic changes in Quaternary sediments of Argentina. Journal of South American Earth Sciences 23, 17–29.
Blanchet, C.L., Thouveny, N., Vidal, L., Leduc, G., Tachikawa, K., Bard, E., Beaufort, L., 2007. Terrigenous input response to glacial/interglacial climatic variations over southern Baja California: a rock magnetic approach. Quaternary Science Reviews 26, 3118–3133.
Blasi, A.M., Zárate, M.A., Kemp, R.A., 2001. Sedimentación y pedogénesis cuaternaria en el noreste de la pampa bonaerense:la localidad Gorina como caso de estudio. Asociación Argentina de Sedimentología, Revista 8, 77–92.
Chen, F.H., Bloemendal, J., Feng, Z.D., Wang, J.M., Parker, E., Guo, Z.T., 1999. East Asian monsoon variations during Oxygen Isotope Stage 5: evidence from the northwest margin of the Chinese loess plateau. Quaternary Science Reviews 18, 1127–1135.
Cruz Jr., F.W., Burns, S.J., Karmann, I., Sharp, W.D., Vuille, M., Ferrari, J.A., 2006. A stalagmite record of changes in atmospheric circulation and soil processes in the Brazilian subtropics during the Late Pleistocene. Quaternary Science Reviews 25, 2749–2761.
Day, R., Fuller, M., Schmidt, V.A., 1977. Hysteresis properties of titanomagnetites: grain-size and compositional dependence. Physics of the Earth and Planetary Interiors 13, 260–267.
Deng, C.L., Vidic, N.J., Verosub, K.L., Singer, M.L., Liu, Q.S., Shaw, J., Zhu, R.X., 2005. Mineral magnetic variation of the Jiaodao Chinese loess/paleosol sequence and its bearing on long-term climatic variability. Journal of Geophysical Research 110 (B03103).
Dunlop, D., Özdemir, Ö, 1997. Rock Magnetism — Fundamentals and Frontiers. Cambridge University Press, New York, NY.
Fidalgo, F., De Francesco, F., Colado, U., 1973. Geología superficial de las hojas Castelli, J.M. Cobo y Monasterio (provincia de Buenos Aires). V Congreso Geológico Argentino 4, 27–39.
Frenguelli, J., 1957. Neozoico, en Geografía de la República Argentina. In: Sociedad Argenntina de estudios Geográficos GAEA, Tomo II tercera parte, Buenos Aires.
Harris, S.E., Mix, A.C., 1999. Pleistocene precipitation balance in the Amazon Basin recorded in deep sea sediments. Quaternary Research 51, 14–26.
Harris, S.E., Mix, A.C., 2002. Climate and tectonic influences on continental erosion of tropical South America, 0–13 Ma. Geology 30, 447–450.
Heller, F., Liu, T.S., 1986. Palaeoclimatic and sedimentary history from magnetic susceptibility of loess in China. Geophysical Research Letters 13, 1169–1172.
Heusser, C.J., 1991. Biogeographic evidence for late Pleistocene palaeoclimate of Chile. Bamberger Geographische Schriften 11, 257–270.
Huybers, P., 2007. Glacial variability over the last two million years: an extended depth-derived age model, continuous obliquity pacing, and the Pleistocene progression. Quaternary Science Reviews 26, 37–55.
Jouzel, J., Masson-Delmotte, V., Catan, O., Dreyfus, G., Falourd, S., Hoffmann, G., Minster, B., Nouet, J., Bartola, J.M., Chappellaz, J., Fischer, H., Gallet, J.C., Johnsen, S., Leuenberger, M., Loulergue, L., Luethi, D., Verter, H., Parrenin, F., Raisbeck, G., Raynaud, D., Schilt, A., Schwander, J., Selmo, E., Souchez, R., Spahni, R., Stauffer, B., Steffensen, J.P., Stenni, B., Stocker, T.F., Tison, J.L., Werner, M., Wolf, E.W., 2007. Orbital and millennial Antarctic climate variability over the past 800,000 years. Science 317, 793–796.
Kämpf, N., Schwertmann, U., 1983. Goethite and hematite in a climosequence in southern Brazil and their application in classification of kaolinitic soils. Geoderma 29, 27–39.
Kemp, R.A., Toms, P.S., Sayago, J.M., Derbyshire, E., King, M., Wagoner, L., 2003. Micromorphology and OSL dating of the basal part of the loess–paleosol sequence at La Mesada in Tucumán province, Northwest Argentina. Quaternary International 106–107, 111–117.
Kemp, R.A., Zárate, M.A., Toms, P., King, M., Sanabria, J., Arguello, G., 2006. Late Quaternary paleosols, stratigraphy and landscape evolution in the Northern Pampa, Argentina. Quaternary Research 66, 119–132.
Kemp, R.A., Zárate, M.A., 2000. Pliocene pedosedimentary cycles in the southern Pampas, Argentina. Sedimentology 47, 3–14.
King, J.W., Banerjee, S.K., Marvin, J., Özdemir, Ö, 1982. A new rock-magnetic approach to selecting sediments for geomagnetic paleointensity studies: application to paleointensity for the last 4000 years. Earth and Planetary Science Letters 59, 404–419.
Kukla, G., An, Z., 1989. Loess stratigraphy in central China. Palaeogeography, Palaeoclimatology, Palaeoecology 72, 203–225.
Lamy, F., Kaiser, J., Ninnemann, U., Hebbeln, D., Arz, H.W., Stoner, J., 2004. Antarctic timing of surface water changes off Chile and Patagonian ice sheet response. Science 304, 1959–1962.
Laskar, J., Robutel, P., Joutel, F., Gastineau, M., Correia, A.C.M., Levrard, B., 2004. A long-term numerical solution for the insolation quantities of the Earth. Astronomy and Astrophysics 428, 261–285. doi:10.1051/0004-6361:20041335.
Lisiecki, L.E., Raymo, M.E., 2005. A Pliocene–Pleistocene stack of 57 globally distributed $\delta^{18}O$ records. Paleoceanography 20 (PA1003). doi:10.1029/2004PA001071.
Liu, X.M., Hesse, P., Béget, J., Rolph, T., 2001. Pedogenic destruction of ferrimagnetics in Alaskan loess deposits. Australian Journal of Soil Research 39, 99–115.

Liu, Q., Deng, C., Torrent, J., Zhu, R., 2007. Review of recent developments in mineral magnetism of the Chinese Loess. Quaternary Science Reviews 26, 368–385.
Liu, X.M., Liu, T.S., Hesse, P., Xia, D.S., Chlachula, J., Wang, G., 2008. Two pedogenic models for paleoclimatic records of magnetic susceptibility from Chinese and Siberian loess. Science in China Series D: Earth Sciences 51, 284–293.
Lu, H., Sun, D., 2000. Pathways of dust input to the Chinese Loess Plateau during the last glacial and interglacial periods. Catena 40, 251–261.
Maher, B.A., 1986. Characterisation of soils by mineral magnetic measurements. Physics of the Earth and Planetary Interiors 42, 76–92.
Maher, B.A., Thompson, R., Zhou, L.P., 1994. Spatial and temporal reconstructions of changes in the Asian paleomonsoon: a new mineral magnetic approach. Earth and Planetary Science Letters 125, 461–471.
Maher, B.A., Alekseev, A., Alekseeva, T., 2002. Variation of soil magnetism across the Russian steppe: its significance for use of soil magnetism as a paleorainfall proxy. Quaternary Science Reviews 21, 1571–1576.
Maher, B.A., Thompson, R., 1995. Paleorainfall reconstructions from pedogenic magnetic susceptibility variations in the Chinese loess and paleosols. Quaternary Research 44, 383–391.
deMenocal, P.B., 1995. Plio-Pleistocene African climate. Science 270, 53–59.
Murad, E., Fischer, W.R., 1988. The geobiochemical cycle of iron. In: Stucki, J.W., et al. (Eds.), Iron in Soils and Clay Minerals. D. Reidel, Dordrecht, The Netherlands, pp. 1–18.
Nabel, P.E., Morras, H.J.M., Petersen, N., Zech, W., 1999. Correlation of magnetic and lithologic features from soils and Quaternary sediments from the undulating Pampa, Argentina. Journal of South American Earth Sciences 12, 311–323.
Ogg, J.G., Smith, A.G., 2004. The geomagnetic polarity timescale. In: Gradstein, F.M., Ogg, J.G., Smith, A.G. (Eds.), A Geologic Time Scale 2004. Cambridge University Press, United Kingdom, pp. 63–86.
Orgeira, M.J., Walther, A.M., Vásquez, C.A., Di Tommaso, I., Alonso, S., Sherwood, G., Yuguan, H., Vilas, J.F.A., 1998. Mineral magnetic record of paleoclimate variation in loess and paleosol from the Buenos Aires formation (Buenos Aires, Argentina). Journal of South American Earth Sciences 11, 561–570.
Peterson, R.G., Stramma, L., 1991. Upper-level circulation in the South Atlantic Ocean. Progress in Oceanography 26, 1–73.
Prohaska, F., 1976. The climate of Argentina, Paraguay and Uruguay. In: Schwerdtfeger, W. (Ed.), World Survey of Climatology: Climates of Central and South America. Elsevier, Amsterdam, pp. 13–112.
Pye, K., 1987. Aeolian Dust and Dust Deposits. Academic Press, New York.
Raymo, M.E., 1994. The initiation of Northern Hemisphere glaciation. Annual Review of Earth and Planetary Sciences 22, 353–383.
Raymo, M.E., Ruddiman, W., Backman, J., Clement, B., Martinson, D., 1989. Late Pleistocene variations in Northern Hemisphere ice sheets and North Atlantic deep water circulation. Paleoceanography 4, 413–446.
Raymo, M.E., Oppo, D., Curry, W., 1997. The mid-Pleistocene climate transition: a deep sea carbon isotopic perspectiva. Paleoceanography 12, 546–559.
Riggi, J.C., Fidalgo, F., Martínez, O., Porro, N., 1986. Geología de los Sedimentos Pampeanos en el partido de la Plata. Revista de la Asociación Geológica Argentina XLIV, 316–333.
Rochette, P., Mathe, P.E., Esteban, L., Rakoto, H., Bouchez, J.L., Liu, Q., Torrent, J., 2005. Non-saturation of the defect moment of goethite and fine-grained hematite up to 57 Teslas. Geophysical Research Letters 32 (L22309) 1-L22309.4.
Ruddiman, W.F., Raymo, M.E., Martinson, D.G., Clement, B.M., Backman, J., 1989. Pleistocene evolution: northern hemisphere ice sheets and north Atlantic Ocean. Paleoceanography 4, 353–412.
Ruddiman, W.F., Janecek, T.R., 1989. Pliocene–Pleistocene biogenic and terrigenous fluxes at equatorial Atlantic Sites 662, 663, and 664. In: Ruddiman, W., Sarnthein, M., et al. (Eds.), Proc. ODP Sci. Results, vol. 108, pp. 211–240. College Station, TX.
Sangode, S.J., Bloemendal, J., 2004. Pedogenic transformation of magnetic minerals in Pliocene–Pleistocene palaeosols of the Siwalik Group, NW Himalaya, India. Palaeogeography, Palaeoclimatology, Palaeoecology 212, 95–118.
Schellenberger, A., Veit, H., 2006. Pedostratigraphy and pedological and geochemical characterization of Las Carreras loess–paleosol sequence, Valle de Tafí, NW-Argentina. Quaternary Science Reviews 25, 811–831.
Schultz, P., Zárate, M., Hames, W., Camilión, C., King, J., 1998. A 3.3 Ma impact in Argentina and possible consequences. Science 282, 2061–2063.
Schulz, M., Mudelsee, M., 2002. REDFIT: estimating red-noise spectra directly from unevenly spaced paleoclimate time series. Computers and Geosciences 28, 421–426.
Schwerdtfeger, W., 1976. Introduction. In: Schwerdtfeger, W. (Ed.), World Survey of Climatology: Climates of Central and South America. Elsevier, Amsterdam, pp. 1–12.
Schwertmann, U., 1988. Occurrence and formation of iron oxides in various pedoenvironments. In: Stucki, J.W., et al. (Eds.), Iron in Soils and Clay Minerals. D. Reidel, Dordrecht, The Netherlands, pp. 267–308.
Smith, J., Vance, D., Kemp, R.A., Archer, C., Toms, P., King, M., Zárate, M., 2003. Isotopic constraints on the source of Argentinian loess – with implications for atmospheric circulation and the provenance of Antarctic dust during recent glacial maxima. Earth and Planetary Science Letters 212, 181–196.
Sun, Y., Clemens, S.C., An, Z., Yu, Z., 2006. Astronomical timescale and palaeoclimatic implication of stacked 3.6-Myr monsoon records from the Chinese Loess Plateau. Quaternary Science Reviews 25, 33–48.
Teruggi, M.E., 1957. The nature and origin of Argentine loess. Journal of Sedimentary Petrology 27, 322–332.
Thompson, F., Oldfield, F., 1986. Environmental Magnetism. Allen & Unwin, London.
Villagrán, C., 1993. Una interpretación climática del registro palinológico del último ciclo glacial–postglacial en Sudamérica. Bull. Inst. Fr. Études Andines 22, 243–258.
Zárate, M.A., 2003. Loess of southern South America. Quaternary Science Reviews 22, 1987–2006.
Zárate, M., Blasi, A., 1993. Late Pleistocene–Holocene Aeolian deposits of the southern Buenos Aires province, Argentina: a preliminary model. Quaternary International 17, 15–20.
Zárate, M., Kemp, R.A., Blasi, A.M., 2002. Identification and differentiation of Pleistocene paleosols in the northern pampas of Buenos Aires, Argentina. Journal of South American Earth Sciences 15, 303–313.
Zárate, M.A., Kemp, R.A., Toms, P.S., 2009. Late Quaternary landscape reconstruction and geochronology in the northern Pampas of Buenos Aires province, Argentina. Journal of South American Earth Sciences 27, 88–99.
Zárate, M., Fasano, J., 1989. The Plio-Pleistocene record of the central eastern pampas, Buenos Aires, Argentina. Palaeogeography, Palaeoclimatology, Palaeoecology 72, 27–52.
Zárate, M., Rabassa, J., 2005. Geomorfología de la provincia de Buenos Aires. In: de Barrio, R., Etcheverry, R., Caballé, M., Llambías, E. (Eds.), Relatorio XVI Congreso Geológico Argentino. Geología y recursos Minerales de la provincia de Buenos Aires, pp. 119–138.
Zhou, L.P., Oldfield, F., Wintle, A.G., Robinson, S.G., Wang, J.T., 1990. Partly pedogenic origin of magnetic variations in Chinese loess. Nature 346, 737–739.
Zinck, J.A., Sayago, J.M., 2001. Climatic periodicity during the late Pleistocene from a loess–paleosol sequence in northwest Argentina. Quaternary International 78, 11–16.